



NRC Publications Archive Archives des publications du CNRC

Controlled synthesis and characterization of Ru-core-Pt-shell bimetallic nanoparticles

Hwang, Bing-Joe; Sarma, Loka Subramanyam; Chen, Ching-Hsiang; Bock, Christina; Lai, Feng-Ju; Chang, Shi-Hong; Yen, Shih-Chieh; Liu, Din-Goa; Sheu, Hwo-Shuenn; Lee, Jyh-Fu

This publication could be one of several versions: author's original, accepted manuscript or the publisher's version. / La version de cette publication peut être l'une des suivantes : la version prépublication de l'auteur, la version acceptée du manuscrit ou la version de l'éditeur.

For the publisher's version, please access the DOI link below. / Pour consulter la version de l'éditeur, utilisez le lien DOI ci-dessous.

Publisher's version / Version de l'éditeur:

<https://doi.org/10.1021/jp807154a>

The Journal of Physical Chemistry C, 112, 50, pp. 19922-19929, 2008-11-19

NRC Publications Record / Notice d'Archives des publications de CNRC:

<https://nrc-publications.canada.ca/eng/view/object/?id=a21bbb1d-3ac8-48f4-97ab-be18ee65b55c>

<https://publications-cnrc.canada.ca/fra/voir/objet/?id=a21bbb1d-3ac8-48f4-97ab-be18ee65b55c>

Access and use of this website and the material on it are subject to the Terms and Conditions set forth at

<https://nrc-publications.canada.ca/eng/copyright>

READ THESE TERMS AND CONDITIONS CAREFULLY BEFORE USING THIS WEBSITE.

L'accès à ce site Web et l'utilisation de son contenu sont assujettis aux conditions présentées dans le site

<https://publications-cnrc.canada.ca/fra/droits>

LISEZ CES CONDITIONS ATTENTIVEMENT AVANT D'UTILISER CE SITE WEB.

Questions? Contact the NRC Publications Archive team at

PublicationsArchive-ArchivesPublications@nrc-cnrc.gc.ca. If you wish to email the authors directly, please see the first page of the publication for their contact information.

Vous avez des questions? Nous pouvons vous aider. Pour communiquer directement avec un auteur, consultez la première page de la revue dans laquelle son article a été publié afin de trouver ses coordonnées. Si vous n'arrivez pas à les repérer, communiquez avec nous à PublicationsArchive-ArchivesPublications@nrc-cnrc.gc.ca.



Controlled Synthesis and Characterization of Ru_{core}–Pt_{shell} Bimetallic Nanoparticles

Bing-Joe Hwang,^{*,†,‡} Loka Subramanyam Sarma,[†] Ching-Hsiang Chen,[†] Christina Bock,[§] Feng-Ju Lai,[†] Shi-Hong Chang,[†] Shih-Chieh Yen,[†] Din-Goa Liu,[‡] Hwo-Shuenn Sheu,[‡] and Jyh-Fu Lee[‡]

Nanoelectrochemistry Laboratory, Department of Chemical Engineering, National Taiwan University of Science and Technology, Taipei 106, Taiwan, National Synchrotron Radiation Research Center, Hsinchu 30076, Taiwan, and National Research Council of Canada, 1200 Montreal Road, Ottawa, Ontario, Canada K1A 0R6

Received: August 11, 2008; Revised Manuscript Received: October 24, 2008

A combined polyol and redox-transmetalation strategy has been proposed to synthesize Ru_{core}–Pt_{shell} bimetallic nanoparticles. By following the in situ X-ray absorption spectroscopy (XAS) at the Pt L_{III} and Ru K edges, the reduction mechanism of Ru nanoparticles (NPs) in tetraethylene glycol (TEG) solutions and the corresponding reaction of Ru NPs with the added Pt²⁺ ions in ethylene glycol (EG) solutions to form Ru_{core}–Pt_{shell} bimetallic nanoparticles was examined. The Pt L_{III}-edge XAS indicates that when the pH of H₂PtCl₆ in EG solution is adjusted to 12 and heated at 80 °C for 5 min, the platinum compound is found to be reduced to a Pt(II) form corresponding to [PtCl₄]²⁻ anionic species. At further reaction time of 10 min, the ligand environment around Pt(II) is changed from Cl⁻ to OH⁻ forming the [Pt(OH)₄]²⁻ species. Analysis of the Ru K-edge XAS results confirms that Ru₃(CO)₁₂ in TEG undergoes a partial decarbonylation when it is heated at 300 °C for 30 min and forms Ru₃(CO)₉ species. At further reaction time of 60 min, Ru₃(CO)₉ species are subjected to a complete decarbonylation to form Ru clusters in TEG solutions. When the EG solution containing [Pt(OH)₄]²⁻ ionic species is mixed with preformed Ru clusters, Pt²⁺ ions are reduced to Pt⁰ on preformed Ru clusters at the expense of Ru via a redox-transmetalation process. The XAS structural parameters suggested that the resulting nanoparticles were of Ru_{core}–Pt_{shell} type structure with a higher extent of atomic distribution of Pt in the cluster when compared with Ru. The unique application of XAS as a fundamental characterization tool to realize the core–shell structure demonstrated here on the Ru–Pt bimetallic system can easily be extended to construct many other types of bimetallic systems for interesting applications.

Introduction

Bimetallic nanoparticles (NPs), either as an alloy or as a core–shell structure, are attracting increasing attention with the growth of interest in nanotechnological disciplines.¹ Among the various types of bimetallic NPs, in particular, core–shell NPs are gaining much importance not only in view of atom economy, which refers to the possibility to substitute the use of noble metals with another less expensive material to make new and affordable catalysts, but also because of their enhanced optical, magnetic, and catalytic properties when compared with their monometallic counterparts.² This enhancement in activity could be explained by electronic, structural, and morphological changes induced in core–shell NPs by their corresponding monometallic NPs. Because of the interesting physicochemical properties of core–shell NPs, methods which can provide growth of one metal onto another in a controlled way and deliberate tailoring of the catalyst nanostructure and characterization methodologies are gaining interest in the contemporary nanoscience research.

A number of synthesis strategies have already been used for the production of core–shell NPs, such as redox-transmetalation,³ ethylene glycol-assisted polyol method,⁴ coreduction,⁵ seed growth method,⁶ and so forth. In order to assess the catalytic

applications of core–shell NPs, rigorous nanoscale characterization techniques are essential. Various techniques, such as transmission electron microscopy (TEM), UV–vis absorption,⁷ resonance light scattering,⁸ surface-enhanced Raman scattering (SERS) techniques, have been proposed for the characterization of core–shell NPs.⁹ Recently, Garcia-Gutierrez et al. have demonstrated that high angle annular dark field (HAADF) technique coupled to a transmission electron microscope is a promising approach to identify the core–shell structures in nanoparticle systems.¹⁰ This technique allows the observation of the interfaces between layers of different elements due to differences in atomic number, densities, or to the presence of strain fields due to differences in lattice parameters so that details of the structure of core–shell type nanoparticles can be obtained. Although a variety of procedures have been employed for the characterization of core–shell nanoparticles, difficulties associated with their usage under in situ conditions have limited their applications. For example, the commonly available X-ray diffraction (XRD) technique may not give real structural information especially at early stages of nanoparticle formation due to its inability to identify the short-range ordering (local environment).¹¹ XRD can provide promising information about the long-range ordering and periodicities preferably on single crystals or polycrystals. Hence, conclusions about the structure or structural evolution of nanosized particles at early stages cannot be simply drawn from XRD. The electron microscopic technique like transmission electron microscopy (TEM)¹² will provide only qualitative understanding of the structure of

* Corresponding author. Fax: +886-2-27376644. E-mail: bjh@mail.ntust.edu.tw.

[†] National Taiwan University of Science and Technology.

[‡] National Synchrotron Radiation Research Center.

[§] National Research Council of Canada.

bimetallic nanoparticles by emphasizing the intensity contrast in nanoparticles. However, usage of TEM to understand the structural evolution at early stages of nanoparticle formation is rather difficult since nanoparticle structure would change during the preparation or transportation of the sample for TEM analysis.

For metal nanoparticles, X-ray absorption spectroscopy (XAS) comprising of X-ray absorption near-edge spectroscopy (XANES) region (conventionally from below the edge up to ~30–50 eV) and extended X-ray absorption fine structure (EXAFS) extending from the XANES region to as high as 2 keV above the edge¹³ has proved to be one of the most suitable methods for investigating structural evolution, and in many cases, structural properties of metal particles can be probed in situ during the different steps of preparation. The XANES spectra provide information about the oxidation state, fractional d-electron density, and electronic environment of the absorbing atom, while the EXAFS spectra yield information on the number, type, and distance of the backscattering atom and allow investigations on the short-range ordering and provide geometric information. In recent years, XAS studies have been well-explored on bimetallic nanoparticles.¹⁴ EXAFS is particularly sensitive to interatomic distances and local disorder and has been successfully utilized to resolve subtle nanoparticle structural details. We have recently made some significant contributions that highlight the applicability of XAS technique to study the nanoparticle formation mechanisms.¹⁵ We also applied XAS to study the chemical transformation of bimetallic nanoparticles to ternary metallic nanoparticles by a cation redox reaction¹⁶ and as a fundamental characterization tool to study the design and controlling the architecture of Pd–Au bimetallic nanoparticles in AOT reverse micelles.¹⁷ These studies are quiet helpful in not only providing detailed knowledge of the particle formation mechanism but also aiding the development of structure-controllable synthesis strategies for metal nanoparticles.

The interest in the controlled synthesis and atomic-level characterization of bimetallic Pt–Ru nanoparticles either in alloy or core–shell structures is increasing because of their application as anode catalysts for the electro-oxidation of methanol in direct methanol fuel cells (DMFCs).¹⁸ The intrinsic properties of PtRu/C NPs are mainly determined by their size, composition, distribution of Pt and Ru sites at the atomic level, homogeneity, and surface population of Pt and Ru.¹⁹ Many synthesis methods appearing in the literature highlight the particle homogeneity as the main criterion in preparing PtRu/C NPs, while some studies focus on the Pt and Ru distribution.²⁰ Recently, Bock et al. reported a polyol process for preparing PtRu/C NPs within the size range of 0.7–4 nm by controlling the pH of the reaction medium in ethylene glycol solutions. In a recent X-ray absorption spectroscopy (XAS) study, we have shown that Pt and Ru atomic distribution in PtRu NPs synthesized by such a polyol process is higher when compared with the conventional colloidal-reduction methodologies, and the particles are of significant stability.²¹ It appeared in the literature that the bimetallic nanoparticles' size and phase ordering will depend on the reaction kinetics which in turn can be controlled by the type of polyol employed in the process.²²

In line with our ongoing effort to establish structure controllable synthesis strategies for bimetallic nanoparticles, we have aimed here to develop a controlled synthesis strategy for Ru_{core}-Pt_{shell} bimetallic nanoparticles and the in situ investigation of the synthesis process by XAS. A combined polyol and redox-transmetalation strategy has been employed to generate Ru_{core}-Pt_{shell} bimetallic NPs. The Pt and Ru atomic distribution

and the structure of the resultant Ru_{core}-Pt_{shell} bimetallic NPs is discussed based on the obtained XAS structural parameters.

Experimental Section

Chemicals. All chemicals were purchased from Acros and were used as received without further purification: hexachloroplatinic acid (H₂PtCl₆·6H₂O, 99.90%), ruthenium dodecarbonyl (Ru₃(CO)₁₂, 99%), ethylene glycol (EG, C₂H₆O₂, 99%), and tetraethylene glycol (TEG, C₆H₁₄O₄, 99%).

Synthesis of Ru_{core}-Pt_{shell} Nanoparticles. For the convenience of XAS measurements to understand the stepwise formation mechanism, the present experiment was designed in three steps.

Step 1. At first, 0.06 M H₂PtCl₆·6H₂O in EG solution was obtained by dissolving appropriate amount of H₂PtCl₆·6H₂O in EG. The pH of this solution was 0.084. Later, the pH of H₂PtCl₆·6H₂O in EG solution was adjusted to 12. The solution was then heated to 80 °C initially for 5 min, and then for 10 min to generate Pt-complex solution containing Pt²⁺ ions.

Step 2. First, an appropriate amount of Ru₃(CO)₁₂ was dissolved in TEG solution at 100 °C under stirring. This solution was initially refluxed at 300 °C for 30 min, and then subjected to further reflux at the same temperature for about 1 h to generate Ru clusters.

Step 3. The solution obtained at step 2 was cooled to 50 °C. Two milliliters of Pt-complex solution obtained at step 1 was added while stirring, and the reaction was continued for 4 h. Further, 3 mL of Pt-complex solution was added and continued the reaction for another 4 h. A redox-transmetalation reaction occurred between the preformed Ru clusters (step 1), and added Pt ions (step 2) will generate Ru_{core}-Pt_{shell} nanoparticles during the step 3. The final product was collected by centrifugation and dried. After each reaction step discussed above, the mixture was cooled to room temperature and subjected to XAS measurements.

High Resolution Transmission Electron Microscopy (HR-TEM) Measurements. HRTEM images were obtained with a JEOL FEI-TEM 2000 instrument operating at an acceleration voltage of up to 200 kV. Samples for HRTEM measurements were prepared by ultrasonically dispersing the nanoparticles in toluene and placing a drop of the colloidal dispersion of nanoparticles on a Cu grid, followed by drying in the oven.

X-ray Absorption Spectroscopy (XAS) Measurements. X-ray absorption measurements were carried out at the Taiwan Beam Line of BL12B2 at the Spring-8, Hyogo, Japan and at the beam line BL01C1 at the National Synchrotron Radiation Research Center, Taiwan. The electron storage ring of Spring-8 was operated at 8 GeV. A double Si(111) crystal monochromator was employed for the energy selection with a resolution $\Delta E/E$ better than 1×10^{-4} at both the Pt L_{III} (11 564 eV) and the Ru K-edges (22 117 eV). Reaction mixtures at different stages of Ru cluster formation, Pt-complex solution, and Ru–Pt nanoparticles formation were brought down to the room temperature and taken in a homemade cell made of PTFE for XAS study. Two holes were made, one on top of the cell and the other on one side. After placing the liquid samples, the top hole was closed with a Teflon rod to avoid the exposure of the sample to the outer atmosphere. A hollow Teflon rod with a Kapton film cap at one end was inserted into the side hole in the in situ XAS cell. The position of the Teflon rod was adjusted to reach the optimum absorption thickness ($\Delta\mu x \approx 1.0$; $\Delta\mu$ is the absorption edge, x is the thickness of the liquid layer) so that the proper edge jump step could be achieved during the measurements. All of the spectra were recorded at room

temperature in a transmission mode. Higher harmonics were eliminated by detuning the double crystal Si(111) monochromator. Three gas-filled ionization chambers were used in series to measure the intensities of the incident beam (I_0), the beam transmitted by the sample (I_s), and the beam subsequently transmitted by the reference foil (I_r). The third ion chamber was used in conjunction with the reference sample, which was a Pt foil for the Pt L_{III}-edge measurements and Ru powder for the Ru K-edge measurements. The control of parameters for EXAFS measurements, data collection modes, and calculation of errors were all done as per the guidelines set by the International XAFS Society Standards and Criteria Committee.²³

X-ray Absorption Spectroscopy (XAS) Data Analysis. The EXAFS data reduction was conducted by utilizing the standard procedures. The EXAFS function, χ , was obtained by subtracting the postedge background from the overall absorption and then normalized with respect to the edge jump step. The normalized $\chi(E)$ was transformed from energy space to k -space, where k is the photoelectron wave vector. The $\chi(k)$ data were multiplied by k^2 to compensate the damping of EXAFS oscillations in the high k -region. Subsequently, k^2 -weighted $\chi(k)$ data in the k -space ranging from 3.6 to 12.6 Å⁻¹ for the Pt L_{III}-edge, from 3.6 to 11.6 Å⁻¹ for the Ru K-edge, were Fourier transformed (FT) to r -space to separate the EXAFS contributions from the different coordination shells. A nonlinear least-squares algorithm was applied to the curve fitting of an EXAFS in the r -space between 0.7 to 3.3 Å for both Pt and Ru depending on the bond to be fitted. For the Pt–Ru reference file, a suitable experimental reference compound was not available for calibration purposes. Hence, the effective scattering amplitude [$f(k)$] and phase shift [$\delta(k)$] for the Pt–Ru was generated by using FEFF7 code by keeping Pt atoms at (0, 1/2, 1/2), (1/2, 0, 1/2), and (1/2, 1/2, 0) and Ru in (0, 0, 0) position in a cubic unit cell of close packing model. The lattice parameter $a = 3.83$ Å is used in the FEFF7 calculation. Reference phase and amplitude for the Pt–Pt and Pt–Cl absorber-scatterer pairs were obtained from a Pt foil and H₂PtCl₆, respectively. For Ru–Ru and Ru–O absorber-scatterer pairs, the phase and amplitude were obtained from the reference Ru powder and RuO₂, respectively. All of the computer programs were implemented in the UWXAFS 3.0 package²⁴ with the backscattering amplitude and the phase shift for the specific atom pairs being theoretically calculated by using the FEFF7 code.²⁵ From these analyses, structural parameters like coordination numbers (N), bond distance (R), the Debye–Waller factor ($\Delta\sigma_j^2$), and inner potential shift (ΔE_0) have been calculated. The amplitude reduction factor (S_0^2) values, which account for the energy loss due to multiple excitations, for Pt and Ru were obtained by analyzing the Pt foil and Ru powder reference samples, respectively, and by fixing the coordination number in the FEFFIT input file. The S_0^2 values were found to be 0.95 and 0.88 for Pt and Ru, respectively. The values of residual factor (R factor) defined by equation 1 are less than 10, indicating that errors associated with data-fitting is quite small.

$$\text{Residual factor (\%)} = \frac{\sum_{i=1}^N |y_{\text{exp}}(i) - y_{\text{theo}}(i)|}{\sum_{i=1}^N |y_{\text{exp}}(i)|} \times 100 \quad (1)$$

The error bounds in the fit parameters N , R , $\Delta\sigma_j^2$, and ΔE_0 were obtained from the 95% confidence level using FEFFIT software. The standard errors (SE) for the coordination numbers at 95% confidence interval were calculated by dividing the error

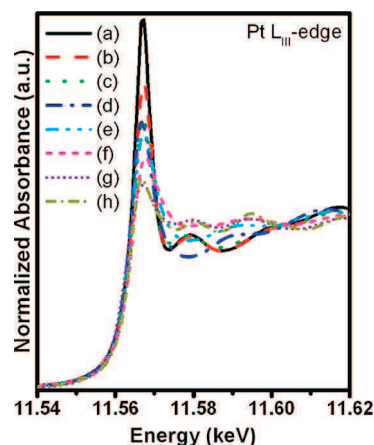


Figure 1. In situ Pt L_{III}-edge XANES spectra for various reaction steps during the formation of Pt–Ru nanoparticles: (a) H₂PtCl₆ in ethylene glycol (EG); (b) H₂PtCl₆ in EG (pH adjusted to 12); (c) H₂PtCl₆ in EG (pH = 12), 80 °C, 5 min; (d) H₂PtCl₆ in EG (pH = 12), 80 °C, 10 min; (e) addition of 2 mL Pt complex in EG to preformed Ru clusters in tetraethylene glycol (TEG) solutions, 50 °C, 4 h; (f) further addition of 3 mL Pt complex in EG to preformed Ru clusters in TEG, 50 °C, 4 h; (g) final Pt–Ru nanoparticles, and (h) the Pt reference foil.

bounds for each coordination number by a factor of 1.96. These standard errors represented for the coordination numbers were used to calculate the standard error for the addition, ratio, and percentage of coordination numbers by employing the appropriate statistical equations. The standard errors calculated for alloying extent of Pt and Ru in final PtRu nanoparticles are well-below that of 15%.

Results and Discussion

X-ray absorption near edge structure (XANES) spectra offers the ability to monitor the changes in oxidation state of the atoms in the material during the course of the reaction. Figure 1 displays the XANES spectra at the Pt L_{III}-edge recorded for all of the reaction steps during the formation of Pt–Ru bimetallic NPs and for the reference Pt foil.

Here, it is clearly seen that the Pt precursor, that is, H₂PtCl₆ in ethylene glycol exhibits a sharp peak positioned at 11.567 keV corresponding to electronic transitions from 2p_{3/2} to unoccupied states above the Fermi level. This sharp peak is generally called a white line, and its magnitude is sensitive to the degree of electron occupancy in the valence orbitals of the absorber.²⁶ In general, if the white line intensity decreases, the density of unoccupied d states is lower and the oxidation state of Pt is lower. As can be seen in Figure 1, the magnitude of white line is decreased when the pH of H₂PtCl₆ in EG is adjusted to 12 indicating the decrease in Pt oxidation state. When H₂PtCl₆ in EG (pH = 12) is heated at 80 °C for 5 min the white line intensity is further decreased. This sharp decrease in white line intensity when compared with the initial state indicates that Pt⁴⁺ ions are reduced to Pt²⁺ ions, and this observation is consistent with our previous study.²¹ No change in white line intensity is observed when H₂PtCl₆ in EG (pH = 12) is continued to heat at 80 °C for 10 min indicating the stability of Pt oxidation state (+2). However, information regarding the ligand environment can not be obtained from XANES measurements alone and it will be confirmed later with EXAFS results. The solution containing Pt²⁺ complex ions in ethylene glycol of this step is cooled down to 50 °C and 2 mL of this solution is added to the solution containing preformed Ru clusters in tetraethylene glycol (TEG). The reaction between the added Pt²⁺

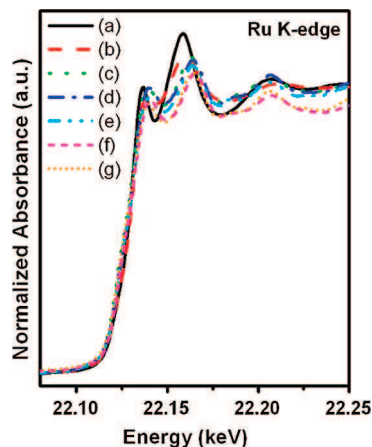


Figure 2. In situ Ru K-edge XANES spectra for various reaction steps during the formation of Pt–Ru nanoparticles. (a) Ru₃(CO)₁₂ in tetraethylene glycol (TEG) at 100 °C; (b) Ru₃(CO)₁₂ in TEG at 300 °C, 30 min; (c) Ru₃(CO)₁₂ in TEG at 300 °C, 60 min (Ru clusters); (d) addition of 2 mL of Pt complex in EG solution to 5 mL solution of Ru clusters in TEG, 50 °C, 4 h; (e) further addition of 3 mL Pt complex in EG to 5 mL solution of preformed Ru clusters in tetraethylene glycol (TEG) solutions, 50 °C, 4 h; (f) final Pt–Ru nanoparticles, and (h) the Ru powder reference.

ions and Ru clusters is continued for 4 h at 50 °C. The purpose of this step is to allow a redox-transmetalation between the added Pt²⁺ ions and the preformed Ru⁰ clusters. In the so-called redox-transmetalation reaction, zero valent Ru nanoparticle, which constitutes the core structure, is partially oxidized while the shell-forming Pt substituent is reduced on the remaining Ru⁰ clusters to generate Ru_{core}-Pt_{shell} nanoparticles. The corresponding XANES scan revealed that the white line intensity is further decreased when compared with the solution containing only Pt²⁺ ions indicating the progressive reduction of Pt²⁺ ions. Further addition of 3 mL complex solution containing Pt²⁺ ions and allowing the reaction to continue for another 4 h witnessed further decrease in the white line intensity. However, its intensity is slightly higher than the white line intensity of the reference Pt foil. This observation indicates that the clusters still possess some Pt-oxidic species. The final product obtained at this step is separated from ethylene glycol and tetraethylene glycol solvents, dried, and subjected to XANES measurements. The corresponding XANES spectra are comparable with that of Pt foil spectra indicating that all of the Pt-oxidic species are reduced to Pt⁰.

Figure 2 shows the Ru K-edge XANES patterns recorded at various steps during the formation of Pt–Ru nanoparticles and the reference Ru powder. A close inspection of the spectra shows that the absorption edge is positioned at 22.10 keV for the beginning compound Ru₃(CO)₁₂ dissolved in tetraethylene glycol (TEG) at 100 °C. However, when Ru₃(CO)₁₂ dissolved in TEG is heated at 300 °C for 30 min, the edge has slightly shifted about 3 eV to a lower energy. This observation indicates the transformation of the metallic state of the Ru–carbonyl complex. Even though the changes which happened at the edge position are subtle, however, the general outlines of the post edge features are very different from each other. This observation may be taken as an indication of disruption of the complex framework. Further increase in the reaction time to 60 min makes the XANES features resemble that of Ru powder reference indicating the formation of Ru clusters in TEG solutions. When 2 mL of the Pt complex solution containing Pt²⁺ ions in EG is added to 5 mL solution of Ru clusters in TEG and allowed to react at 50 °C for 4 h, the edge energy

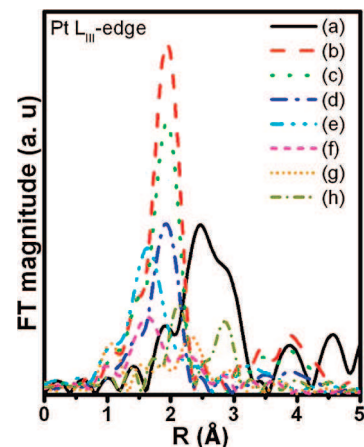


Figure 3. Pt L_{III}-edge FT-EXAFS spectra (k^2 weighted) for various reaction steps during the formation of Pt–Ru nanoparticles. (a) The Pt reference foil; (b) H₂PtCl₆ in ethylene glycol (EG); (c) H₂PtCl₆ in EG (pH adjusted to 12); (d) H₂PtCl₆ in EG (pH = 12), 80 °C, 5 min; (e) H₂PtCl₆ in EG (pH = 12), 80 °C, 10 min; (f) addition of 2 mL Pt complex in EG to preformed Ru clusters in tetraethylene glycol (TEG) solutions, 50 °C, 4 h; (g) further addition of 3 mL Pt complex in EG to preformed Ru clusters in TEG, 50 °C, 4 h; and (h) final Pt–Ru nanoparticles.

position is slightly shifted to higher levels when compared with the Ru powder reference. This observation indicates that Ru clusters are oxidized and a redox-transmetalation between Ru clusters and the added Pt²⁺ ions has occurred to generate Ru_{core}-Pt_{shell} NPs. However, it is difficult to confirm the core–shell structure of Ru–Pt NPs at this stage, and it will be discussed in detail in the next section of EXAFS results. The XANES spectra of final Pt–Ru NPs after filtration and drying are closely matched with the XANES spectra of Ru reference powder consistent with a metallic state.

In order to achieve better structural information of species formed at various reaction steps during the formation of Ru_{core}-Pt_{shell} nanoparticles, the Pt L_{III}-edge Fourier transformed (FT) $k^2\chi(k)$ extended X-ray absorption fine structure (EXAFS) spectrum is recorded at the various reaction steps during the formation of Pt–Ru NPs and is shown in Figure 3. The best fit EXAFS parameters (N , coordination number; R , bond distance; σ^2 , Debye–Waller factor; ΔE_0 , inner potential shift) are summarized in Table 1. The FT of the Pt precursor, that is, H₂PtCl₆ in EG exhibits a strong peak at 2.0 Å characteristic of the presence of a Pt–Cl bond. The position and nature of the peak and the number of chlorine atoms are found to be comparable to the earlier studies.²⁷ Adjusting the pH of H₂PtCl₆ in EG to 12 decreases the magnitude of the Pt–Cl peak suggesting that there is a change in the local environment of Pt⁴⁺ ions. The important result is that a sharp decrease in the Pt–Cl peak magnitude is observed when the H₂PtCl₆ in EG (pH = 12) solution is heated at 80 °C for 5 min. The contribution of a Pt–Cl peak with an average coordination number of 3.8 at a distance of 2.31 Å suggests that Pt⁴⁺ ions of H₂PtCl₆ are reduced to Pt²⁺ ions at this step consistent with XANES observations.

At further reaction times, that is, for 10 min, the FT peak shifted to lower R values and signature of the Pt–Cl bonding has completely disappeared. The appearance of the Pt–OH bond was found as evidenced from N_{Pt-O} of 3.84 and R_{Pt-O} of 2.04 Å at this stage. The obtained XAS parameters at this step are near the values calculated for [Pt(OH)₄]²⁻ species.^{15b} When 2 mL of the Pt complex solution containing [Pt(OH)₄]²⁻ species is added to the solution containing preformed Ru clusters and

TABLE 1: Best Fit Parameters Obtained from the Analysis of the Pt L_{III}-edge EXAFS Spectra of Various Reaction Steps During the Formation of Pt–Ru NPs^a

reaction state	shell	<i>N</i>	<i>R</i> (Å)	σ^2 ($\times 10^{-3}$) (Å ²)	ΔE_0 (eV)	<i>R</i> factor
H ₂ PtCl ₆ in EG	Pt–Cl	5.64 (±0.10)	2.33 (±0.010)	2.7	8.8	0.011
H ₂ PtCl ₆ in EG (pH = 12)	Pt–Cl	4.94 (±0.12)	2.33 (±0.012)	4.1	8.7	0.021
H ₂ PtCl ₆ in EG (pH = 12), 80 °C, 5 min	Pt–Cl	3.81 (±0.10)	2.31 (±0.010)	4.5	8.7	0.016
H ₂ PtCl ₆ in EG (pH = 12), 80 °C, 10 min	Pt–OH	3.84 (±0.10)	2.04 (±0.010)	5.4	8.5	0.011
Add 2 mL Pt complex to Ru clusters, 50 °C, 4 h	Pt–OH	1.84 (±0.11)	2.02 (±0.012)	4.9	9.3	
	Pt–Ru	0.28 (±0.12)	2.71 (±0.014)	12.9	22.2	
	Pt–Pt	4.04 (±0.17)	2.78 (±0.017)	12.7	2.9	0.018
Further add 3 mL Pt complex to Ru clusters, 50 °C, 4 h	Pt–OH	2.20 (±0.19)	2.74 (±0.016)	4.4	9.1	
	Pt–Ru	0.71 (±0.22)	2.71 (±0.017)	11.9	20.1	
	Pt–Pt	4.41 (±0.24)	2.78 (±0.017)	11.7	3.3	0.038
RuPt powder (Ru _{0.9} Pt _{0.1})	Pt–Ru	1.11 (±0.11)	2.71 (±0.012)	2.5	3.7	
	Pt–Pt	5.84 (±0.14)	2.75 (±0.012)	6.3	6.0	0.004

^a *N*, coordination numbers; *R_j* (Å), coordination distances; σ_j^2 (Å²), Debye–Waller factors; ΔE_0 (eV), inner potential correction.

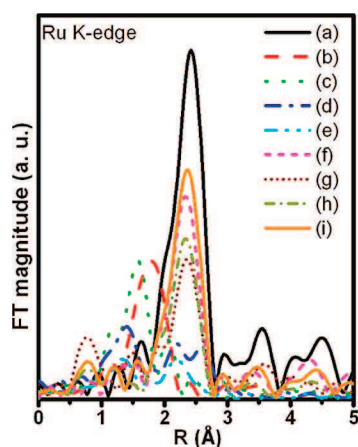


Figure 4. Ru K-edge FT-EXAFS spectra (k^2 weighted) for various reaction steps during the formation of Pt–Ru nanoparticles. (a) Ru powder reference; (b) RuCl₃; (c) Ru(OH)₂; (d) Ru₃(CO)₁₂ in tetraethylene glycol (TEG) at 100 °C; (e) Ru₃(CO)₁₂ in TEG at 300 °C, 30 min; (f) Ru₃(CO)₁₂ in TEG at 300 °C, 60 min (formation of Ru clusters); (g) addition of 2 mL of Pt complex in EG solution to 5 mL solution of Ru clusters in TEG, 50 °C, 4 h; (h) further addition of 3 mL Pt complex in EG to 5 mL solution of preformed Ru clusters in TEG solutions, 50 °C, 4 h, and (i) final Pt–Ru nanoparticles.

allowed to react for 4 h, the magnitude of the Pt–OH bond signal is decreased, and the Pt–Pt and Pt–Ru bonding signatures begin to appear between 2 to 3 Å. Further addition of 3 mL Pt complex solution leads to an increase in the formation of Pt–Ru particles as suggested by the increase in N_{Pt-Ru} and N_{Pt-Pt} to 0.71 and 4.41, respectively, compared with the previous step. However, still the Pt-oxidic species are retained in the sample as suggested from the presence of Pt–OH bond in FT-EXAFS spectra. The sample obtained at this step was filtered and dried and subjected to XAS analysis. In the corresponding FT-EXAFS spectra (scan h of Figure 3), a complete removal of the Pt–OH and increase in the magnitude of Pt–Pt and Pt–Ru correlations were found.

Figure 4 represents the FT-EXAFS spectra at the Ru K-edge during the formation of Ru clusters from Ru₃(CO)₁₂ in TEG solutions and Pt–Ru clusters via the redox-transmetalation reaction between preformed Ru clusters and added Pt²⁺ ions in EG solutions. As can be seen from Figure 4, the peak in the range $1.0 < R/\text{Å} < 3.0$ is attributable to a three shell Ru–Ru, Ru–C, and Ru(–C–)O contributions. Since the Ru(–C–)O contribution was found to be strongly coupled with the Ru–Ru contribution, these two contributions had to be analyzed simultaneously. Table 2 lists the results of the data analysis for Ru₃(CO)₁₂ in TEG solutions, Ru clusters, and Pt–Ru clusters.

The intensity of the peak appeared in the range $1.0 < R/\text{Å} < 3.0$ is decreased when Ru₃(CO)₁₂ in TEG solutions is heated at 300 °C for 30 min which may be attributable to the loss of carbonyl ligands from the clusters. However, after heating Ru₃(CO)₁₂ in TEG solutions at 300 °C for 60 min, intensity of the peak at higher *R* values, that is, between 2 to 3 Å, increased drastically, and a complete absence of the peak at lower *R* values was found. The data indicate a Ru–Ru coordination number of 6.54 with an average distance of 2.67 Å. These observations indicate the formation of Ru clusters after the complete removal of carbonyl ligands. Addition of Pt complex solution containing Pt²⁺ ions to Ru clusters decreases the FT magnitude of the peak appeared between 2 and 3 Å with a splitting. The peak splitting is related to the first coordination shell of RuPt and is caused by interference between the backscattering from Ru and from Pt neighbors indicating the formation of Pt–Ru clusters.²⁸ A new peak between 0.5 and 2 Å corresponding to Ru–Cl begins to appear, indicating the oxidation of Ru clusters has taken place during the redox-transmetalation process. Further addition of Pt²⁺ ions increases the magnitude of FT peak related Pt–Ru clusters (2~3 Å). However, the Ru–Cl signature is still retained in the cluster. After the sample is subjected to filtration and drying, the contribution from Ru–Cl bonding completely disappears.

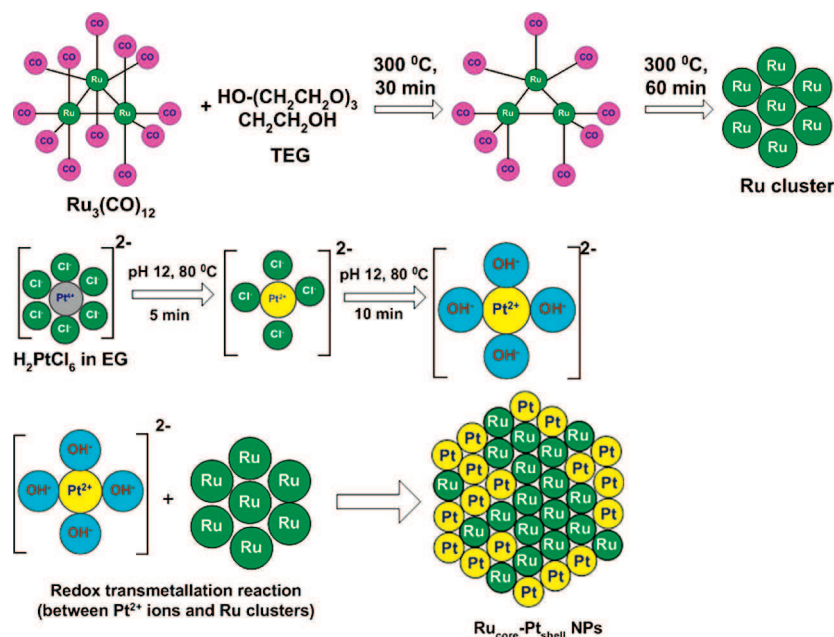
Formation of Ru_{core}–Pt_{shell} Bimetallic Nanoparticles. On the basis of the XAS results, we have attempted to discuss the formation mechanism of Ru_{core}–Pt_{shell} bimetallic NPs. By comparing the XAS spectra and fitting results of both the Pt L_{III} edge and the Ru K-edge, a model is proposed for the mechanism of Ru_{core}–Pt_{shell} bimetallic NPs formation and is shown in Scheme 1. From the Ru K-edge XAS, for the beginning compound Ru₃(CO)₁₂ in TEG solution heated at 100 °C, we found a Ru–Ru coordination number of 2.04 with an average distance of 2.81 Å, a Ru–C coordination number of 3.96 at an average distance of 1.95 Å, a Ru(–C–)O coordination number of 7.95 at an average distance of 3.15 Å, and Ru–O coordination number of 4.03 at an average distance of 3.15 Å. The fitting model of Ru₃(CO)₁₂ is based on *Ibam* space group. These results indicate that there is no change in the Ru₃(CO)₁₂ cluster framework at this temperature. Upon increasing the temperature to 300 °C and maintaining it for 30 min, there is a complete absence of the Ru(–C–)O coordination, and the N_{Ru-C} , N_{Ru-Ru} , and N_{Ru-O} are found to be 2.84, 1.83, and 2.79, respectively. The loss of 7.95 Ru(–C–)O coordination indicates that, on average, three CO ligands are removed from the Ru₃(CO)₁₂ cluster during the decarbonylation, and these results indicate that the species obtained at this stage are in the form of Ru₃(CO)₉. The observed decarbonylation is further

TABLE 2: Best Fit Parameters Obtained from the Analysis of the Ru K-edge EXAFS Spectra of Various Reaction Steps During the Formation of Pt–Ru NPs^a

reaction state	shell	<i>N</i>	<i>R</i> (Å)	σ^2 ($\times 10^{-3}$) (Å ²)	ΔE_0 (eV)	<i>R</i> factor
Ru ₃ (CO) ₁₂ in TEG, 100 °C	Ru–C	3.96 (±0.18)	1.99(±0.012)	3.0	–0.5	0.018
	Ru–Ru	2.04 (±0.21)	2.81 (±0.014)	6.6	–27.0	
	Ru–O	4.03 (±0.22)	3.15 (±0.012)	1.3	–6.4	
	Ru–C–O	7.95 (±0.18)	3.15 (±0.012)	5.4	–5.7	
Ru ₃ (CO) ₁₂ in TEG react at 300 °C, 30 min	Ru–C	2.84 (±0.24)	1.86 (±0.016)	4.5	–10.8	0.025
	Ru–Ru	1.83 (±0.14)	2.75 (±0.012)	7.3	–27.8	
	Ru–O	2.79 (±0.23)	3.08 (±0.012)	1.5	–14.1	
Ru ₃ (CO) ₁₂ in TEG react at 300 °C, 60 min Add 2 mL Pt complex to Ru clusters, 50 °C, 4 h	Ru–Ru	6.54 (±0.10)	2.67 (±0.008)	5.1	–8.2	0.007
	Ru–Cl	0.86 (±0.16)	2.21 (±0.011)	0.0	–17.8	
	Ru–Ru	4.85 (±0.13)	2.67 (±0.010)	5.7	–8.5	
	Ru–Pt	0.11 (±0.11)	2.71 (±0.014)	0.0	8.8	
Further add 3 mL Pt complex to Ru clusters, 50 °C, 4 h	Ru–Cl	1.11 (±0.12)	2.22 (±0.008)	0.0	–17.6	0.021
	Ru–Ru	4.39 (±0.09)	2.67 (±0.007)	4.0	–8.2	
	Ru–Pt	0.21 (±0.2)	2.71 (±0.004)	0.0	9.0	
RuPt powder (Ru _{0.9} Pt _{0.1})	Ru–Ru	8.30 (±0.09)	2.68 (±0.009)	5.6	–4.8	0.004
	Ru–Pt	0.12 (±0.10)	2.71 (±0.010)	2.5	3.7	

^a *N*, coordination numbers; *R_j* (Å), coordination distances; σ_j^2 (Å²), Debye–Waller factors; ΔE_0 (eV), inner potential correction.

SCHEME 1: Schematic of Formation of Ru_{core}-Pt_{shell} Bimetallic Nanoparticles by a Polyol Assisted Redox Transmetalation Strategy



evidenced from the decrease in the Ru–Ru bond distance by 0.21 Å when compared with the values characterizing the fully carbonylated cluster precursor consistent with the literature studies.²⁹ Increasing the reaction time to 60 min produces a Ru–Ru coordination of 6.54 with an average distance of 2.67 Å indicating the formation of Ru clusters. From the Pt L_{III} edge XAS, for H₂PtCl₆ in ethylene glycol solution, we found Pt–Cl coordination of 5.64 at an average distance of 2.33 Å, and it shows that the Pt⁴⁺ ion is surrounded by nearly six chloride ions consistent with our previous observations.²¹ Upon adjusting the pH of H₂PtCl₆ in EG solution, the Pt–Cl coordination number is decreased to 4.94 indicating the beginning of the loss of Cl[–] ligands around the Pt⁴⁺ ion. Heating the H₂PtCl₆ in EG solution at 80 °C for 5 min produces the Pt–Cl coordination number (*N*_{Pt–Cl}) and the Pt–Cl interatomic distance (*R*_{Pt–Cl}) 3.81 and 2.31 Å, respectively, and are consistent with the constants related to anionic PtCl₄^{2–} ions.³⁰ However, after the heating time is increased to 10 min, the ligand environment around Pt²⁺ ion is changed from Cl[–] to OH[–]. The *N*_{Pt–OH} and *R*_{Pt–OH} are found to be 3.84 and 2.04 Å, respectively, consistent with the constants

related to Pt(OH)₄^{2–} ions.^{15b} When the solution containing Pt(OH)₄^{2–} ions is added to the preformed Ru clusters and allowed to react at 50 °C for 4 h, the *N*_{Pt–OH} is decreased to 1.84 and produced a Pt–Ru coordination of 0.28 at an average distance of 2.71 Å. The *N*_{Pt–Pt} is found to be 4.04 at this stage. The corresponding Ru K-edge XAS data suggest that Ru–Cl coordination of 0.86 at an average distance of 2.21 Å is found. The *N*_{Ru–Ru} and *N*_{Ru–Pt} are found to be 4.85 and 0.11, respectively. These results indicate that most of the Pt(OH)₄^{2–} ions are reduced to form Pt through the sacrificial oxidation of the zerovalent ruthenium atoms and simultaneously deposited on the surface of Ru cores. Meanwhile, the Ru atoms are oxidized to Ru³⁺, and the electron transfer between the two metals results in core–shell type nanoparticles. Further addition of Pt(OH)₄^{2–}

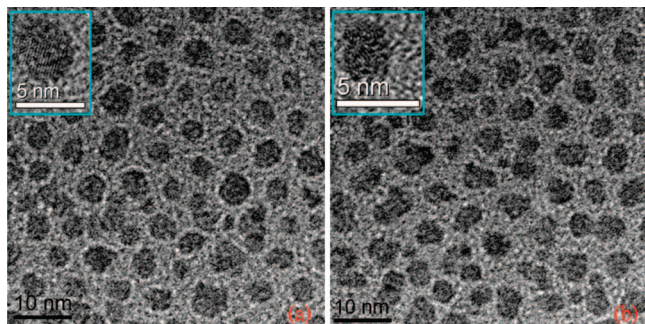


Figure 5. High resolution TEM (HRTEM) images of (a) bare Ru nanoparticles before treatment with Pt^{2+} ions, and (b) final $\text{Ru}_{\text{core}}\text{-Pt}_{\text{shell}}$ nanoparticles formed after treating bare Ru nanoparticles with Pt^{2+} ions via a galvanic redox transmetalation reaction.

ions increases the extent of redox-transmetalation and corresponding formation of $\text{Ru}_{\text{core}}\text{-Pt}_{\text{shell}}$ nanoparticles as realized from the Pt L_{III}-edge and Ru K-edge XAS parameters. At this step, from the Pt L_{III}-edge XAS data, the $N_{\text{Pt-Ru}}$ and $N_{\text{Pt-Pt}}$ are found to be 0.71 and 4.41, respectively. Similarly, from the Ru K-edge XAS data, the $N_{\text{Ru-Ru}}$ and $N_{\text{Ru-Pt}}$ are found to be 4.39 and 0.21, respectively. However, still we find the Pt-OH and Ru-Cl coordination at this step, and these contributions are eliminated only after filtration and drying the nanoparticles. XAS measurements on the final Ru-Pt nanoparticles produced Pt and Ru coordination around Pt of 5.84 and 1.11, respectively. Similarly, Pt and Ru coordination around Ru is found to be 0.12 and 8.30, respectively. The coordination number derived from XAS is a strong and nonlinear function of the particle diameter up to 3–5 nm. This property has been widely used in EXAFS analysis to determine the size of the nanoparticle.¹⁹ In the present study, for the final $\text{Ru}_{\text{core}}\text{-Pt}_{\text{shell}}$ NPs the number of nearest neighbors around Ru and Pt are 8.42 and 6.95, respectively, giving an averaged first-shell coordination number of 7.68. This value corresponds to an average particle size of about 1.5–2 nm on the assumption of a close-packed structure.³¹

In order to verify the particle sizes of Ru nanoparticles before treatment with Pt^{2+} ions and after treatment with Pt^{2+} ions, HRTEM analyses were performed. The corresponding HRTEM images of bare Ru nanoparticles before treatment with Pt^{2+} ions and after treatment with Pt^{2+} ions are shown in panels a and b, respectively, of Figure 5. The HRTEM image of as-prepared Ru nanoparticles shown in Figure 5a indicates that the Ru clusters are well-dispersed on a TEM grid with an average diameter of about 5 nm. The average diameter of final $\text{Ru}_{\text{core}}\text{-Pt}_{\text{shell}}$ nanoparticles obtained after treating the preformed Ru nanoparticles with the added Pt^{2+} ions is of about 4 nm. The decrease in particle diameter may be caused due to the etching effect and/or reaction stoichiometry between metal nanoparticles and metal ions which is considered to be typical for some galvanic replacement reactions.³² However, the particle size obtained through HRTEM measurements for final $\text{Ru}_{\text{core}}\text{-Pt}_{\text{shell}}$ nanoparticles (ca. 4 nm) is comparatively higher than that of the particle size calculated through XAS measurements (ca. 1.5–2 nm). This observation may be caused by the aggregation of nuclei due to the drying process during HRTEM observation and consistent with our previous findings.^{15b}

It has been shown in the previous reports that, for a homogeneous system of A–B bimetallic NPs for which the core of the cluster is composed of N atoms of A (N_{A}) and the surface is made of N atoms of B (N_{B}), the total coordination number ($N_{\text{AA}} + N_{\text{AB}}$) for the A atom is greater than the total coordination for the B atoms ($N_{\text{BA}} + N_{\text{BB}}$).³³ For the final Pt–Ru NPs of the

present study, the total coordination number of Pt and Ru around Ru ($\Sigma N_{\text{Ru-i}} = N_{\text{Ru-Ru}} + N_{\text{Ru-Pt}}$) is found to be 8.42, and it is greater than that of the total coordination number of Pt and Ru around Pt ($\Sigma N_{\text{Pt-i}} = N_{\text{Pt-Pt}} + N_{\text{Pt-Ru}}$) calculated as 6.95. The observed parameter relationship, that is, $\Sigma N_{\text{Ru-i}} > \Sigma N_{\text{Pt-i}}$, indicated a core–shell structure for the synthesized Pt–Ru NPs consisting of a Ru-rich core and Pt-rich shell. Since the atomic distribution and alloying extent of Pt and Ru in the Pt–Ru NPs plays a significant role in assessing their catalytic activity, we attempted to discuss these properties based on XAS methodology developed previously in our group.³⁴ The parameter which describes the atomic distribution of Pt in the cluster is termed as “ P_{observed} ” and is defined as a ratio of $N_{\text{Pt-Ru}}/(N_{\text{Pt-Pt}} + N_{\text{Pt-Ru}})$. Similarly, “ R_{observed} ” which has a meaning of atomic distribution of Ru in the cluster is defined as a ratio of $N_{\text{Ru-Pt}}/(N_{\text{Ru-Ru}} + N_{\text{Ru-Pt}})$. In the present study for the final Pt–Ru NPs, the atomic distribution structural parameters P_{observed} and R_{observed} was calculated as 0.12 and 0.01, respectively. From the P_{observed} and R_{observed} parameters, we can calculate alloying extent of Pt (J_{Pt}) and Ru (J_{Ru}) values by using eqs 2 and 3 respectively.

$$J_{\text{Pt}} = \frac{P_{\text{Observed}}}{P_{\text{Random}}} \times 100 \quad (2)$$

$$J_{\text{Ru}} = \frac{R_{\text{Observed}}}{R_{\text{Random}}} \times 100 \quad (3)$$

where P_{random} and R_{random} can be taken as 0.5 for perfect alloyed bimetallic NPs if the atomic ratio of Pt and Ru is 1:1. This value can be achieved by assuming $N_{\text{Pt-Pt}} = N_{\text{Pt-Ru}}$ and $N_{\text{Ru-Ru}} = N_{\text{Ru-Pt}}$ which is generally true for the perfectly alloyed bimetallic NPs. By using eqs 2 and 3, the alloying extent of Pt (J_{Pt}) and Ru (J_{Ru}) values are calculated as 24 and 2% respectively. Both the observed parameter relationships $\Sigma N_{\text{Ru-i}} > \Sigma N_{\text{Pt-i}}$ and $J_{\text{Pt}} > J_{\text{Ru}}$ further supports that the obtained Pt–Ru NPs adopt a Ru-rich core and Pt-rich shell structure. The higher value of P_{observed} , 0.12 and J_{Pt} , 24% indicates the higher extent of atomic distribution or alloying extent of Pt atoms when compared with Ru. This observation also indicates that a considerable amount of hetero metallic Pt–Ru bonds may exist either in the shell region or in the interface region of core–shell NPs. In contrast, the very low P_{observed} and J_{Ru} values suggest that Ru is largely dominated in the core region and homo-metallic Ru–Ru bonds are preferred rather than hetero-metallic Ru–Pt bonds. The observed results are reasonable since the reduction of the added Pt^{2+} ions and corresponding oxidation of preformed Ru nanoparticles were confined to the vicinity of the Ru particles surface. The overall XAS results suggest that the obtained nanoparticles are consistent with a Ru core and a Pt shell nanostructure.

Conclusions

The present study concludes that a combined polyol and redox-transmetalation strategy is effective for the formation of core–shell nanostructures. The in situ investigation of the synthesis of Ru–Pt nanoparticles by X-ray absorption spectroscopy analysis confirms that these nanoparticles presented a $\text{Ru}_{\text{core}}\text{-Pt}_{\text{shell}}$ structure. By using the experimental XAS data, we are able to propose a detailed model for the formation of $\text{Ru}_{\text{core}}\text{-Pt}_{\text{shell}}$ bimetallic nanoparticles. On the basis of the XAS structural parameters, we found that the atomic scale distribution of Pt is much better than that of Ru, whereas in the case of Ru segregation effect dominates in the $\text{Ru}_{\text{core}}\text{-Pt}_{\text{shell}}$ bimetallic nanoparticles. The fact that the added Pt^{2+} ions are reduced at the expense of core Ru atoms to form $\text{Ru}_{\text{core}}\text{-Pt}_{\text{shell}}$ NPs suggests

that one can control the thickness of the Pt-shell by properly choosing the particle size of core Ru atoms and the amount of added Pt²⁺ ions, and such efforts are currently under progress in our laboratory. We believe that such an optimization of the Ru-Pt system may yield more active electrocatalysts for fuel cell applications.

Acknowledgment. The authors gratefully acknowledge the financial support from the National Science Council (NSC-95-2120-M-011-002 and NSC-95-2221-E-011-130), facilities from the National Synchrotron Radiation Research Center (NSRRC), and the National Taiwan University of Science and Technology.

References and Notes

- (1) (a) Zhou, B.; Hermans, S.; Somorjai, G. A. *Nanotechnology in Catalysis*; Kluwer Academic/Plenum Publishers: New York, 2004. (b) Schmid, G. *Chem. Rev.* **1992**, *92*, 1709. (c) Daniel, M.-C.; Astruc, D. *Chem. Rev.* **2004**, *104*, 293.
- (2) (a) Templeton, A. C.; Wuelfing, W. P.; Murray, R. W. *Acc. Chem. Res.* **2000**, *33*, 27–36. (b) Caruso, F. *Adv. Mater.* **2001**, *13*, 11–22. (c) Zhong, C.-J.; Maye, M. M. *Adv. Mater.* **2001**, *13*, 1507–1511.
- (3) (a) Chen, D.; Li, J.; Shi, C.; Du, X.; Zhao, N.; Sheng, J.; Liu, S. *Chem. Mater.* **2007**, *19*, 3399–3405. (b) Lee, W. R.; Kim, M. G.; Choi, J. R.; Park, J. I.; Ko, S. J.; Oh, S. J.; Cheon, J. *J. Am. Chem. Soc.* **2005**, *127*, 16090. (c) Park, J. I.; Kim, M. G.; Jun, Y. W.; Lee, J. S.; Lee, W. R.; Cheon, J. *J. Am. Chem. Soc.* **2004**, *126*, 9072. (d) Park, J. I.; Cheon, J. *J. Am. Chem. Soc.* **2001**, *123*, 5743.
- (4) Harpness, R.; Gedanken, A. *Langmuir* **2004**, *20*, 3431–3434.
- (5) Nath, S.; Praharaj, S.; Panigrahi, S.; Ghosh, S. K.; Kundu, S.; Basu, S.; Pal, T. *Langmuir* **2005**, *21*, 10405–10408.
- (6) Srnová-Šloufová, I.; Vičková, B.; Bastl, Z.; Hasslet, T. *Langmuir* **2004**, *20*, 3407–3415.
- (7) (a) Yonezawa, T.; Toshima, N. *J. Mol. Catal.* **1993**, *83*, 167. (b) Henglein, A. *J. Phys. Chem. B* **2000**, *104*, 2201.
- (8) Chen, L.; Zhao, W.; Jiao, Y.; He, X.; Wang, J.; Zhang, Y. *Spectrochim. Acta Part A: Mol. Biomol. Spectrosc.* **2007**, doi:10.1016/j.saa.2006.12.014.
- (9) Hu, J.-W.; Li, J.-F.; Ren, B.; Wu, D.-Y.; Sun, S.-G.; Tian, Z.-Q. *J. Phys. Chem. C* **2007**, *111*, 1105–1112.
- (10) Garcia-Gutierrez, D.; Gutierrez-Wing, C.; Miki-Yoshida, M.; Jose-Yacamán, M. *Appl. Phys. A: Mater. Sci. Process.* **2004**, *79*, 481–487.
- (11) Cao, D.; Bergens, H. *J. Power Sources* **2004**, *134*, 170.
- (12) Ashcroft, A. T.; Cheetham, A. K.; Harris, P. J. F.; Jones, R. H.; Natarajan, S.; Sankar, G.; Stedman, N. J.; Thomas, J. M. *J. Catal. Lett.* **1994**, *24*, 47.
- (13) Rehr, J. J.; Albers, R. C. *Rev. Mod. Phys.* **2000**, *72*, 621.
- (14) (a) Camara, G. A.; Giz, M. J.; Paganin, V. A.; Ticianelli, E. A. *J. Electroanal. Chem.* **2002**, *537*, 21. (b) Russell, A. E.; Rose, A. *Chem. Rev.* **2004**, *104*, 4613. (c) Hills, C. W.; Nashner, M. S.; Frenkel, A. I.; Shapley, J. R.; Nuzzo, R. G. *Langmuir* **1999**, *15*, 690. (d) Toshima, N.; Harada, M.; Yamazaki, Y.; Asakura, K. *J. Phys. Chem.* **1992**, *96*, 9927. (e) Toshima, N.; Harada, M.; Yonezawa, T.; Kushihashi, K.; Asakura, K. *J. Phys. Chem.* **1991**, *95*, 7448. (f) Bian, C.-R.; Suzuki, S.; Asakura, K.; Ping, L.; Toshima, N. *J. Phys. Chem. B* **2002**, *106*, 8587.
- (15) (a) Hwang, B.-J.; Tsai, Y.-W.; Sarma, L. S.; Tseng, Y. L.; Liu, D. G.; Lee, J. F. *J. Phys. Chem. B* **2004**, *108*, 10427. (b) Tsai, Y.-W.; Tseng, Y. L.; Sarma, L. S.; Liu, D.-G.; Lee, J.-F.; Hwang, B.-J. *J. Phys. Chem. B* **2004**, *108*, 8148. (c) Chen, C. H.; Sarma, L. S.; Wang, G. R.; Chen, J. M.; Shih, S. C.; Tang, M. T.; Liu, D. G.; Lee, J. F.; Chen, J. M.; Hwang, B. J. *J. Phys. Chem. B* **2006**, *110*, 10287. (d) Chen, C. H.; Hwang, B. J.; Wang, G. R.; Sarma, L. S.; Tang, M. T.; Liu, D. G.; Lee, J. F. *J. Phys. Chem. B* **2005**, *109*, 21566.
- (16) Wang, D.-Y.; Chen, C.-H.; Yen, H.-C.; Lin, Y.-L.; Huang, P.-Y.; Hwang, B.-J.; Chen, C.-C. *J. Am. Chem. Soc.* **2007**, *129*, 1538.
- (17) Chen, C.-H.; Sarma, L. S.; Chen, J.-M.; Shih, S.-C.; Wang, G.-R.; Liu, D.-G.; Tang, M.-T.; Lee, J.-F.; Hwang, B.-J. *ACS Nano* **2007**, *1*, 114.
- (18) (a) Bock, C.; Paquet, C.; Couillard, M.; Botton, G. A.; MacDougall, B. R. *J. Am. Chem. Soc.* **2004**, *126*, 8028. (b) Hogarth, M. P.; Hards, G. A. *Platinum Met. Rev.* **1996**, *40*, 150.
- (19) Frenkel, A. I.; Wills, C. W.; Nuzzo, R. G. *J. Phys. Chem. B* **2001**, *105*, 12689.
- (20) Hwang, B.-J.; Chen, C.-H.; Sarma, L. S.; Chen, J.-M.; Wang, G.-R.; Tang, M.-T.; Liu, D.-G.; Lee, J.-F. *J. Phys. Chem. B* **2006**, *110*, 6475.
- (21) Sarma, L. S.; Chen, C.-H.; Kumar, S. M. S.; Wang, G.-R.; Yen, S.-C.; Liu, D.-G.; Sheu, H.-S.; Yu, K.-L.; Tang, M.-T.; Lee, J.-F.; Bock, C.; Chen, K.-H.; Hwang, B.-J. *Langmuir* **2007**, *23*, 5802.
- (22) (a) Jeyadevan, B.; Hobo, A.; Urakawa, K.; Chinnasamy, C. N.; Shiroda, K.; Tohji, K. *J. Appl. Phys.* **2003**, *93*, 7574. (b) Chinnasamy, C. N.; Jeyadevan, B.; Shiroda, K.; Tohji, K. *J. Appl. Phys.* **2003**, *93*, 7583. (c) Jeyadevan, B.; Urakawa, K.; Hobo, A.; Chinnasamy, C. N.; Shiroda, K.; Tohji, K.; Djayaprawira, D. D.; Tsunoda, M.; Takahashi, M. *Jpn. J. Appl. Phys.* **2003**, *42*, L350.
- (23) (a) See for example the guidelines for data collection modes for EXAFS measurements and user controlled parameters: http://ixs.iit.edu/subcommittee_reports/sc/sc00report.pdf. (b) See for example the guidelines for errors reporting: http://ixs.iit.edu/subcommittee_reports/sc/err-rep.pdf.
- (24) Stern, E. A.; Newville, M.; Ravel, B.; Yacoby, Y.; Haskel, D. *Physica B* **1995**, *208–209*, 117.
- (25) Zabinsky, S. I.; Rehr, J. J.; Anukodinov, A. L.; Albers, R. C.; Eller, M. J. *Phys. Rev. B* **1995**, *52*, 2995.
- (26) (a) McBreen, J.; Mukerjee, S. *J. Electrochem. Soc.* **1995**, *142*, 3399. (b) Min, M.-K.; Cho, J.; Cho, K.; Kim, H. *Electrochim. Acta* **2000**, *45*, 4211.
- (27) Ayala, R.; Sánchez Marcos, E.; Díaz-Moreno, S.; Armando Solé, V.; Muñoz-Páez, A. *J. Phys. Chem. B* **2001**, *105*, 7598.
- (28) McBreen, J.; Mukerjee, S. *J. Electrochem. Soc.* **1995**, *142*, 3399.
- (29) Alexeev, O. S.; Graham, G. W.; Shleif, M.; Adams, R.; Gates, B. C. *J. Phys. Chem. B* **2002**, *106*, 4697.
- (30) Wyckoff, R. W. G. *Crystal Structure*, 2nd ed.; Interscience Publishers: New York, 1965; Vol. 3, p 69.
- (31) (a) Gates, B. C.; Katzer, J. R.; Schuit, G. C. *Chemistry of Catalytic Process*; McGraw-Hill: New York, 1979. (b) Greigor, R. B.; Lytle, F. W. *J. Catal.* **1980**, *63*, 476.
- (32) Shon, Y.-S.; Dawson, G. B.; Porter, M.; Murray, R. W. *Langmuir* **2002**, *18*, 3880.
- (33) (a) Via, G. H.; Sinfelt, J. H.; Iwasawa, Y., Eds; *X-ray Absorption Fine Structure for Catalysts and Surfaces*; World Scientific: London, 1996. (b) Bazin, D.; Sayers, D.; Rehr, J. J. *J. Phys. Chem.* **1997**, *101*, 11040.
- (34) Hwang, B.-J.; Sarma, L. S.; Chen, J.-M.; Chen, C.-H.; Shih, S.-C.; Wang, G.-R.; Liu, D.-G.; Lee, J.-F.; Tang, M.-T. *J. Am. Chem. Soc.* **2005**, *127*, 11140.